Long-wave infrared surface plasmon grating coupler

Justin W. Cleary,[1] Gautam Medhi,[1] Robert E. Peale,[1,*] and Walter R. Buchwald[2]

[1]Department of Physics, University of Central Florida, Orlando, Florida 32816, USA

[2]Air Force Research Laboratory, Sensors Directorate, Hanscom Air Force Base, Massachusetts 01731, USA

*Corresponding author: peale@mail.ucf.edu

Received 1 March 2010; revised 29 April 2010; accepted 4 May 2010; posted 4 May 2010 (Doc. ID 124819); published 28 May 2010

We present a simplified analytic formula that may be used to design gratings intended to couple long-wave infrared radiation to surface plasmons. It is based on the theory of Hessel and Oliner (1965). The recipe is semiempirical, in that it requires knowledge of a surface-impedance modulation amplitude, which is found here as a function of the grating groove depth and the wavelength for silver lamellar gratings at CO_2 laser wavelengths. The optimum groove depth for photon-to-surface-plasmon energy conversion was found by experiment and calculation to be ~10%–15% of the wavelength. This value is about twice what has been reported previously in the visible spectral range for sinusoidal grating profiles.

OCIS codes: 240.6680, 050.2770, 250.5403, 260.3060.

1. Introduction

Gratings are key in proposed nanophotonic integrated circuits for both the incoupling of free electromagnetic waves into bound surface plasmon polaritons (SPP) and the outcoupling of SPPs into freely propagating optical fields. Proper grating design is essential in order to achieve efficient couplers that provide good beam profiles [1]. This paper considers the effects of wavelength and grating amplitude for lamellar gratings (rectangular-groove profiles) on SPP generation. Most SPP studies have been at visible and near IR frequencies, but long-wave IR (LWIR) is emphasized here [2,3].

Photon-SPP coupling for Ag sinusoidal gratings of different amplitudes has been studied experimentally in [4,5] at visible wavelengths. In [4], SPPs were excited by electron beams, and the angular position and angular width of outcoupled light at a given wavelength was recorded. In [5], specular reflection of monochromatic light from gratings revealed dips at certain angles of incidence when light energy was converted to SPPs. Shifts and broadening of the angular resonances with increasing grating amplitudes up to about 10% of λ were reported, but there was no comparison to theory. Hutley and Bird [6], observing absorption resonances in diffracted light for nominally sinusoidal gratings of amplitude in the range 0.12 λ to 0.7 λ, also reported broadening and shifts. The present LWIR study is of gratings with amplitude in the range 0.01 λ to 0.5 λ.

A number of similar experiments, complemented by numerical simulations, reported effects of grating amplitude on angle or wavelength of resonances in reflection from metallic or dielectric gratings of various morphologies [7–11]. The longest wavelength in any of these studies was 5 μm [8]. Goals of the present paper include the extension of grating couplers to the LWIR, where the permittivity is significantly different than at wavelengths ≤5 μm and to demonstrate a simple analytic formula useful for the design and optimization of grating couplers.

The most widely cited analytic formulation of the grating coupler problem is that of Hessel and Oliner [12]. A review of all 323 citations of [12] indicates that apparently no application of that formulation to experimental results or SPP coupler design has been published. The formulas are, in fact, somewhat complicated, but this paper demonstrates certain

0003-6935/10/163102-09$15.00/0

simplifications that facilitate relatively simple calculations of angular resonance spectra. These simplified calculations agree adequately with experiments on lamellar gratings in the 6–10 μm wavelength range, at least for engineering purposes. Though broadening is adequately represented in the calculations, the theory does not predict the small but definite angular shift that occurs with increasing grating amplitude, unless the permittivity is adjusted to account for the increasing surface porosity. These shifts, however, amount to only three-tenths of a degree at the maximum grating amplitude deemed usable for an SPP coupler and, thus, likely will have little impact on SPP coupler applications.

An essential parameter in the theory is the surface-impedance modulation index, M, which is an unspecified function of grating amplitude, wavelength, permittivity, and geometry of the grating. We present empirical values for the modulation index determined by fitting the theory to experimental data for the wavelengths and grating amplitudes investigated here. M is found to vary linearly with wavelength. M varies as a second-order polynomial with grating amplitude up to amplitude values that are still useful for plasmon couplers.

It is possible to obtain a more accurate description of experimental observations using numerical methods [13–16]. However, it may be difficult to obtain intuitive understanding or interpretation of the observed phenomena without running numerous numerical experiments. Moreover, the codes elaborated from rigorous scattering theories are generally part of very expensive commercial software packages, the learning curve for the use of such packages is steep, and the physics behind the code is often obscure. Hence, there is value in having, as an alternative, simple approximate analytic formulas that optical engineers may use to design a reasonably effective grating coupler.

2. Experiment

Gratings were formed by evaporation of Ag through a photolithographic mask on top of a 200 nm evaporated Ag film supported by a polished silicon substrate. The supporting Ag film is optically thick in the IR. The period of all gratings was 20 μm and the duty cycle was 50%, but the grating amplitude was varied by varying the evaporation time. Measured profiles (KLA-Tencor) determine the peak-to-peak amplitude h of the gratings and confirm that the grating lines have sharp square edges. IR ellipsometry was completed using a J.A. Woollam IR-VASE on optically thick Ag films deposited by the same procedure without the use of the mask [17].

The gratings were mounted and aligned on a motorized goniometer. Specular reflection of p-polarized radiation (electric field E in the plane of incidence) from a CO_2 laser (9.250 and 10.591 μm wavelength) was collected by a power meter P as a function of the angle of incidence θ, as indicated schematically in Fig. 1. Similar measurements were made on the same gratings using a quantum cascade laser (6.14 μm wavelength) and a 77 K HgCdTe detector. Generation of SPPs was indicated by loss of power in the reflected beam for a narrow range of θ.

To confirm the generation of propagating SPPs at the resonance angle, some samples were prepared with a second grating separated by 1 cm from the first, also indicated schematically in Fig. 1. An IR camera, C, was set up to image this second grating, while all rays from the first grating were blocked from reaching the camera by a screen. With the goniometer, it was convenient to observe the $n = 1$ outcoupled beam, which propagates in a direction parallel to the specularly reflected beam at an outcoupling angle of θ. No attempt was made to observe the other expected outcoupled beams.

3. Theoretical Considerations

Hessel and Oliner [12] describe two types of resonances, the usual Rayleigh type, corresponding to the emergence or exit of a diffraction order at grazing incidence, and a type associated with leaky surface waves supported by the grating. The latter are SPPs. They are leaky because they propagate across a modulated surface that leads to outcoupling back into free photons. For metal gratings of rectangular profile in the LWIR, both resonance types coincide to within 0.02% of the incidence angle.

The theory of Hessel and Oliner [12] models the grating as a modulated surface impedance, $Z(x)$, where x is the coordinate in the plane of the grating and perpendicular to the grooves [Fig. 1]. For purposes of obtaining and testing simple design formulas, only the first Fourier component of that modulation is retained here, as represented by

$$Z(x) = Z_0\left(1 + M\cos\left[\frac{2\pi x}{d}\right]\right), \tag{1}$$

even though the actual gratings have rectangular ridges containing many higher harmonics. The full theory of [12] is more general. The effect of neglecting the higher harmonics is to eliminate higher order SPP

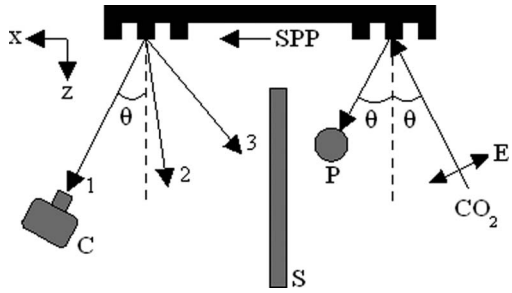

Fig. 1. Schematic of experiment: p-polarized CO_2 laser radiation is incident on the right grating, and specular reflection is monitored as a function of angle of incidence using power meter P. A second grating 1 cm to the left outcouples the SPP that has traveled to it, and this event is imaged with an infrared camera C. The screen S prevents any rays from the first grating from reaching the camera.

resonances from the calculated angular reflectance spectra. In Eq. (1), M is the modulation index (some function of grating permittivity, amplitude, and wavelength) and the grating period is d. The limit for zero modulation is given by

$$Z_0 = \sqrt{\frac{\mu_0}{(\varepsilon' + \varepsilon'')\varepsilon_0}} = \frac{377\ \Omega}{\sqrt{\varepsilon' + \varepsilon''}}, \tag{2}$$

where μ_0, ε_0, and 377 Ω are, respectively, the permeability, permittivity, and impedance of free space, while ε' and ε'' are the real and imaginary parts of the relative permittivity for the metal. Equation (1) suggests that the average permittivity is also Z_0, but we note that bulk permittivity values in Z_0 may need to be replaced by effective values for a corrugated surface. For metals in the infrared, we have $\varepsilon'' \ll |\varepsilon'|$ and $\varepsilon' < 0$, giving for the relative surface impedance

$$\zeta \equiv \frac{Z_0}{377\ \Omega} \approx \frac{-i}{\sqrt{|\varepsilon'|}}. \tag{3}$$

If the imaginary part cannot be neglected, and with $\varepsilon' = -|\varepsilon'|$, we have

$$\zeta = -i(\ |\varepsilon'|^2 + \varepsilon''^2)^{-1/4}\left\{\cos\left(\frac{\phi}{2}\right) + i\sin\left(\frac{\phi}{2}\right)\right\}, \tag{4}$$

where $\phi = \tan^{-1}(\varepsilon''/|\varepsilon'|)$. The experimentally determined permittivity values for our silver films are given in Table 1, together with relative surface-impedance values from Eqs. (3) and (4).

The magnetic field of the incident p-polarized wave is $H\exp[i(k_s x - \kappa_0 z)]$, where the in-plane wavevector k_s is related to the incidence angle by $k_s = k\sin(\theta)$, and $k = 2\pi/\lambda$. The field of the scattered wave is

$$H_s(x,z) = \sum_{n=-\infty}^{\infty} I_n \exp\left[i\left(k_s + \frac{2\pi n}{d}\right)x + i\kappa_n z\right], \tag{5}$$

where I_n is the complex amplitude of the nth spectral order (propagating or not) and

$$\kappa_n = \sqrt{k^2 - \left(k_s + \frac{2\pi n}{d}\right)^2}. \tag{6}$$

Note that n is an integer taking both positive and negative values. For sufficiently large n, k_n is purely imaginary, the nth Fourier component is exponentially damped in the direction normal to the surface, and no diffracted spectral order is present. Otherwise, κ_n is purely real, giving the usual propagating spectral orders of the grating. The vanishing of κ_n, or identically, the condition for the nth diffracted beam to occur at ±90°, is known as the Rayleigh condition [18] and is the cause of one type of the so-called Wood's anomalies [19]. Here, propagating spectral orders either emerge or disappear. The diffraction equation, $d(\sin\theta_n - \sin\theta) = n\lambda$ (θ_n and θ are both positive when on the opposite sides of the normal), gives the Rayleigh condition as $\sin(\pm\pi/2) - \sin(\theta) = n\lambda/d$, which, when satisfied, results in a redistribution of energy among the various orders, including the zeroth (specular) order I_0. The second form of the so-called Woods's anomalies is a resonance phenomenon, which will now be discussed in terms of the work of Hessel and Oliner [12]. For the geometry previously discussed, the reflectivity, R, is given by

$$R = \left|\frac{I_0}{H}\right|^2 = \left|\frac{2D_0 - 4/M}{D_0 + A_1 + B_{-1}} - 1\right|^2, \tag{7}$$

with

$$D_n = \frac{2}{M}\left[1 + \frac{\kappa_n}{\zeta\, k}\right], \tag{8}$$

$$A_1 = -\{D_1 - [D_2 - (D_3 - \ldots)^{-1}]^{-1}\}^{-1}, \tag{9}$$

$$B_{-1} = -\{D_{-1} - [D_{-2} - (D_{-3} - \ldots)^{-1}]^{-1}\}^{-1}. \tag{10}$$

Equations (9) and (10) are continued fractions. If, at a certain angle, D_1 or D_{-1} becomes small, the other D_n remain large, so that the approximation $A_1 \approx -1/D_1$ and $B_{-1} \approx -1/D_{-1}$ can be made in Eqs. (9) and (10). This leads to the following approximation for specular reflection

$$R \approx \left|\frac{2D_0 - 4/M}{D_0 - \frac{1}{D_1} - \frac{1}{D_{-1}}} - 1\right|^2, \tag{11}$$

which is valid for the conditions of our experiment. When D_1 reaches a minimum, a dip in specular reflection will occur. The behavior of D_1 is determined by two complex values, namely, the relative surface impedance ζ and κ_1. We have

$$\mathrm{Re}[D_1] = \frac{2}{M}\left[1 + \frac{\zeta'\,\kappa_1}{|\zeta|^2 k}\right], \tag{12}$$

and (with $\zeta'' = -|\zeta''|$ for metals)

$$\mathrm{Im}[D_1] = \frac{2|\zeta''|\kappa_1}{M|\zeta|^2 k}. \tag{13}$$

Table 1. Optical Parameters of Ag

	$\lambda(\mu\mathrm{m})$	$-\varepsilon'$	ε''	ζ [Eq. (3)]	ζ [Eq. (4)]
Ag	6.14	2707 ± 270	469 ± 80	$-i0.0192$	$-i(0.0190 + i0.0016)$
	9.250	5397 ± 330	1463 ± 120	$-i0.0136$	$-i(0.0133 + i0.0018)$
	10.591	6774 ± 450	1971 ± 300	$-i0.0121$	$-i(0.0118 + i0.0017)$

As the incidence angle θ increases from 0, the Rayleigh condition $\kappa_1 = 0$ is eventually reached, where the $n = 1$ diffracted order goes off at grazing angle. Before this occurs, κ_1 is real, both parts of D_1 are positive and slowly varying, and no resonance behavior occurs in this angular regime. When the incidence angle passes the Rayleigh condition for $n = 1$, κ_1 is pure imaginary and can be written as $\kappa_1 = i|\kappa_1|$. Then

$$\mathrm{Im}[D_1] = \frac{2\zeta'|\kappa_1|}{M|\zeta|^2 k}, \tag{14}$$

which is always positive, and

$$\mathrm{Re}[D_1] = \frac{2}{M}\left[1 - \frac{|\zeta''|\ |\kappa_1|}{|\zeta|^2 k}\right]. \tag{15}$$

Equation (15) will go to zero, and the specular reflection will reach a minimum, when $|\zeta''|\ |\kappa_1| = |\zeta|^2 k$. This immediately leads to the condition for resonance-type anomalies in terms of the relative surface impedance as

$$\sin(\theta) + \frac{\lambda}{d} = \sqrt{1 + \frac{|\zeta|^4}{|\zeta''|^2}}. \tag{16}$$

A feature of the observed reflection anomalies is their asymmetry. To clarify the origin of asymmetry in the resonance line shapes, Eq. (7) is rewritten in terms of the real and imaginary parts of each of the complex factors as

$$R = \frac{(D_0' + A_1' + B_{-1}')^2 + \left(\frac{4\cos(\theta)}{M|\zeta|} - D_0'' - A_1'' - B_{-1}''\right)^2}{(D_0' + A_1' + B_{-1}')^2 + (D_0'' + A_1'' + B_{-1}'')^2}. \tag{17}$$

In Eq. (17), ζ is taken to be purely imaginary as in Eq. (3). The vanishing of D_1 causes a derivative-like resonance line shape in A_1' and an asymmetric peak in A_1'', while all other factors in Eq. (17) vary slowly with θ.

When more terms are kept in the continued fractions of Eqs. (9) and (10), progressively weaker resonances can be observed whenever $D_n = 0$. The weakening of the resonances with increasing order results from the neglect of higher harmonics in the Fourier expansion of the grating [Eq. (1)], but including these harmonics results in a much more complicated formula for R. Consequently, we limit our calculations to the $n = 1$ resonance, although our experiments reveal also the $n = -3$ resonance. This should still permit adequate SPP coupler design.

According to the discussion above, minima in R [Eq. (11)] occur when D_1' [Eq. (15)] becomes small. The vanishing of D_1' with the approximation Eq. (3) gives the condition for "guided surface wave" generation, namely

$$\sin(\theta) + \frac{\lambda}{d} = \sqrt{\frac{|\varepsilon'| - 1}{|\varepsilon'|}}. \tag{18}$$

This "guided surface wave" must be identified with the SPP of modern literature, because their wavefunctions are the same [12,20]. The usual expression [20] for the launching of an SPP by a grating is

$$\sin(\theta) + \frac{n\lambda}{d} = \pm\mathrm{Re}\left[\sqrt{\frac{\varepsilon}{\varepsilon + 1}}\right] = \pm\frac{c}{\omega}\mathrm{Re}[k_{\mathrm{spp}}], \tag{19}$$

where k_{spp} is the complex SPP wavevector and n is an integer of either sign. Our experiment considers only positive angles of incidence θ.

Equations (18) and (19) give resonance angles that differ by an insignificant 0.001% for Ag gratings. Figure 2 presents a graphical representation of the SPP resonance condition of Eq. (19) as it pertains to our experiment. The horizontal axis is the real part of the SPP wavevector, or the component of the incident photon wavevector in the plane of the grating. The vertical axis is the SPP photon energy. The solid lines are SPP dispersion curves, which are close to, but fall below the grazing-incidence light line with slope $\hbar c$. The dashed curves are light lines with slope $\hbar c \sin(\theta)$. All incident angles in our experiment are on the same side of the surface normal and are thus positive, giving positive slopes. The origins of the dashed curves are shifted by integer multiples of the grating momentum $k_g = 2\pi/d$. The shifted light lines intersect the SPP dispersion curves at energies corresponding to the two CO_2 laser wavelengths used in this work, as indicated. The angles of incidence necessary for an intersection at the proper CO_2 photon energy determine the positions of the resonance absorptions, where SPPs are generated. These angles θ, determined from Eq. (19) for curves a, b, a', b', are 32.5°, 22.8°, 28.1°, and 36.1°, respectively. Note that,

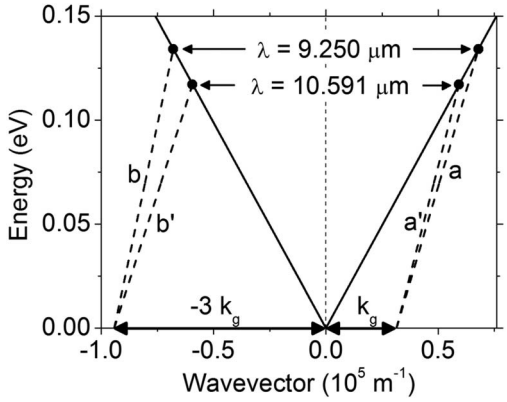

Fig. 2. Graphical representation of the SPP resonance conditions of this experiment. Solid curves are silver SPP dispersion curves. Light curves (dashed) for different angles of incidence and shifted by different integer multiples of grating momentum are shown. The points of intersection establish the conditions for SPP generation at the wavelengths indicated. Angles of incidence for a, b, a', and b' are 32.5°, 22.8°, 28.1°, and 36.1°, respectively.

for the intersections with curves b and b', the SPP momentum is negative while the in-plane component of the incident photon is always positive.

4. Results

The experiment represented by the Fig. 1 schematic was performed, and outcoupled light was imaged with the IR camera as coming from the second grating when incoming p-polarized light is incident on the first grating at the resonance angle determined by Eq. (19) for $n = 1$. This confirms the generation of a propagating SPP. The light outcoupled at the second grating was confirmed to be highly directional. It was not a diffuse scattering and could only be observed when the IR camera was precisely positioned at the expected outcoupling angle. With the goniometer at the $n = 1$ incoupling resonance, it was inconvenient to observe outcoupled beams for $n \neq 1$, and these were not looked for. The calculated characteristic propagation length for SPPs on noble metals at the CO_2 laser is ~1 cm [3], which is the same as the distance between the two gratings. In samples for which the separation was 2 cm, no outcoupled light from the second grating was detected.

For the $n = -3$ incoupling resonance, the generated SPP propagates opposite to the direction of the in-plane component of the incident wavevector [Fig. 2]. It was experimentally inconvenient to observe outcoupled radiation at a second grating placed to the right of the first [according to Fig. 1]. Consequently, generation and propagation of an $n = -3$ SPP was not directly confirmed by observations. This higher order SPP generation was inferred from the observed dip in reflection from the first grating.

Figure 3 (inset) presents a measured Ag-grating profile before (thin curve) and after (thick curve) it was annealed for 30 s at 850 °C. Before annealing, the profile is rectangular. After annealing, the profile has become more sinusoidal, except for small bumps on the edges of each line. Figure 3 presents the Fourier transform of the grating profiles in the inset (including additional periods), with labeled peaks corresponding to the multiples of the fundamental spatial frequency. The as-deposited profile (thin curve) has clear Fourier components up to six times the fundamental. The annealed profile (thick curve) has mainly the fundamental, with a small contribution at five times the fundamental to account for the bumps on the edges. Notable for the experiments reported here is that the peak corresponding to three times the fundamental is strongly attenuated by annealing. As will be shown, the effect is to strongly reduce the SPP coupling for $n = -3$. Note that the strength of the fundamental is also reduced by annealing, which has the effect of reducing the $n = 1$ SPP coupling.

Figure 4 presents the reflected intensity as a function of angle of incidence for the Ag grating with 1 μm amplitude, before (thin curve) and after (thick curve) annealing, for two different CO_2 laser wavelengths. Two resonances are observed at each wavelength, corresponding to different amounts of grating momentum added to allow generation of a surface plasmon. A third resonance predicted near normal incidence is inaccessible to the experiment. Calculated resonance angles θ from Eq. (19) with permittivity values from Table 1 are indicated by symbols. The observed resonances are labeled by the corresponding n value from Eq. (19). These resonances are approximately symmetrical about the Littrow angle $\sin\theta_L = -m\lambda/2d$ for $m = -2$, similar to [6]. The $n = -3$ resonance corresponds to an SPP momentum that is opposite the in-plane component of the incident photon momentum [Fig. 2].

The unrepeatable sloping baselines in Fig. 4, due to laser power drift, can be ignored. Otherwise, the baseline at the Littrow angle is higher (lower) for λ/d greater than (less than) the value 1/2, as was noted in [6]. If $\lambda/d = 1/2$, we would have the $n = +3$ and -1 diffraction orders passing simultaneously off the grating horizon for $\theta = 30°$. We have chosen λ/d valves on either side of the value 1/2. As θ sweeps through the range of observation for $\lambda/d > 1/2$, the number of allowed diffracted orders (not including spectral reflection), changes from 3 to 2 and back

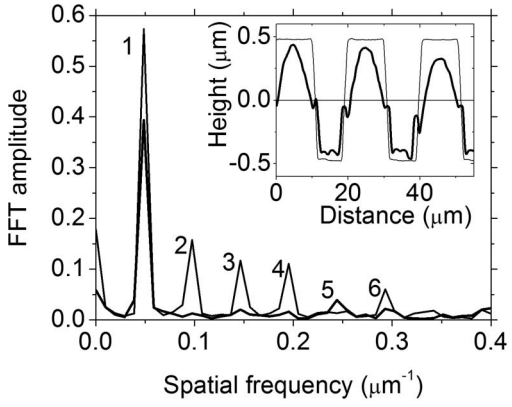

Fig. 3. Fourier transform of a measured profile (inset) for as-deposited (thin curve) and annealed (thick curve) Ag gratings with amplitude of 1 μm.

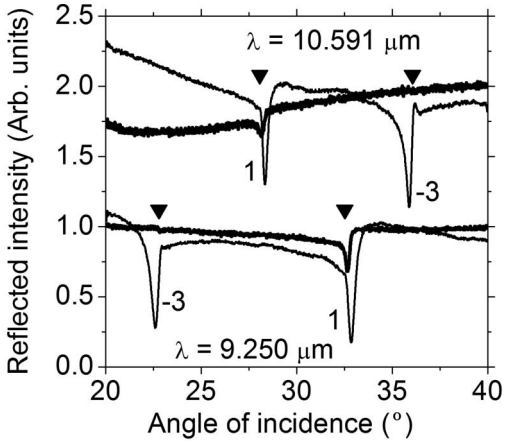

Fig. 4. Angular reflectance spectrum for as-deposited (thin curve) and annealed (thick curve) Ag grating with amplitude of 1 μm at two different CO_2 wavelengths.

to 3. This explains why the power in the specular beam is higher in the central region, where the total outcoupled power is shared only among two spectral orders as opposed to three. When $\lambda/d < 1/2$, the number of diffracted orders follows the sequences $3 \rightarrow 4 \rightarrow 3$, so that the opposite situation holds for the specular intensity when compared to the previous case.

From Fig. 4 it is clear that, first, the $n = -3$ resonance nearly disappears for the annealed sample. Second, the $n = 1$ resonance is reduced in amplitude. Third, the resonance angle undergoes a small shift, with the positions for the annealed sample being closer to the calculated positions. Fourth, the $n = -3$ resonance angle exceeds the $n = 1$ resonance angle at the 10.591 μm excitation wavelength, while the opposite is true for the 9.250 μm excitation wavelength.

Figure 5 presents the experimental reflected intensity at the two different CO_2 laser wavelengths for gratings of different amplitude h. For $h = 100$ nm, absorption resonances were observed to be at the same level as the background noise. Discernible resonances first appear weakly at $h = 200$ nm, where the $n = 1$ resonances occur at 32.58° and 28.14° for $\lambda = 9.250$ and 10.591 μm, respectively. These values are in good agreement with those calculated from Eq. (19) of 32.52° and 28.07°, with the discrepancy possibly due to systematic error from the estimate of the origin of the angle scale. The resonances are deepest at $h = 1$ μm, but by 2 μm they are strongly deformed and broadened. As in Fig. 4, the $n = 1$ and $n = -3$ resonances switch places when the wavelength is changed from one extreme value of the CO_2 laser range to the other. The $n = 1$ resonance is always sharpest on the side of low angles, and the baseline of the reflection is lower on that side. For $n = -3$, the opposite holds.

Figure 6 presents calculated resonance spectra, according to Eq. (11). Because a sinusoidal surface-impedance variation is assumed with no higher harmonics [Eq. (1)], we see only the $n = 1$ resonance,

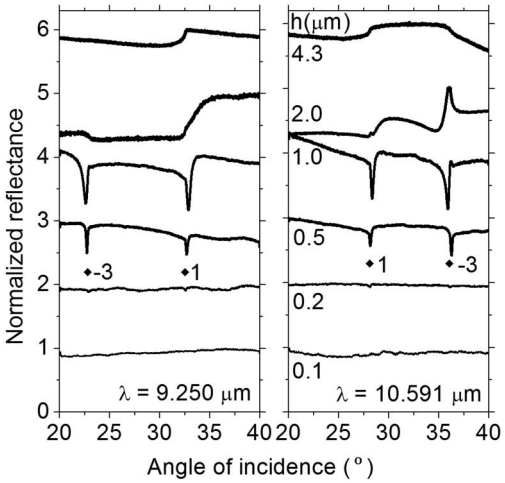

Fig. 5. Measured angular reflectance for two different p-polarized CO_2 laser wavelengths and Ag gratings with different amplitudes.

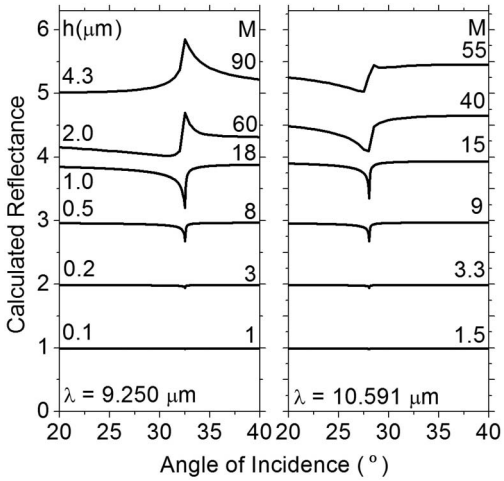

Fig. 6. Calculated angular reflectance for Ag gratings of different amplitudes.

as in Fig. 4, for the annealed grating. The observed resonance peaks for the smallest h value are 32.52° and 28.07°, in exact agreement with the values calculated from Eq. (19). In this figure the surface-impedance modulation amplitude M was the only fitting parameter, and its value was adjusted until the calculated curves had the best qualitative agreement with the observed curves. For $h \leq 1$ μm, the depth of the resonance was the main factor in judging the goodness of the fit. For $h > 1$ μm, the lines are distorted, so that other considerations, such as the amplitude of the baseline on either side of the resonance, came into play. Notable differences between theory and experiment are in the upward spikes and the absence of any shift in the theoretical resonance positions with increasing h. For grating depths up to ~10% of the LWIR wavelengths, the angle at which the reflectance minimum occurs is described by the surface plasmon resonance condition to within a few tenths of a degree.

The Hessel and Oliner [12] theory predicts very sharp features with widths less than 0.05° that we do not observe experimentally. Thus, for our calculation, we have chosen a step size of 0.05°, which seems reasonable as a bound on the angular resolution of our experiments. The sharpest features observed have widths of about 0.2°. The sharp calculated features broaden at grating amplitudes ≥2 μm such that an angular resolution of 0.5° was required to eliminate them. This suggests that these sharp structures may be theoretical artifacts.

Figure 7 (inset) compares, in detail, the calculated and observed resonances for $h = 0.5$ μm and $\lambda = 10.591$ μm. Curve shape and depth were the primary considerations in judging the fit. Because the theory fails to account for the shift that occurs with increasing h, the calculation is shifted horizontally by ~0.1° to match the data. Because the experiment does not give absolute reflectance, the calculation is also shifted vertically.

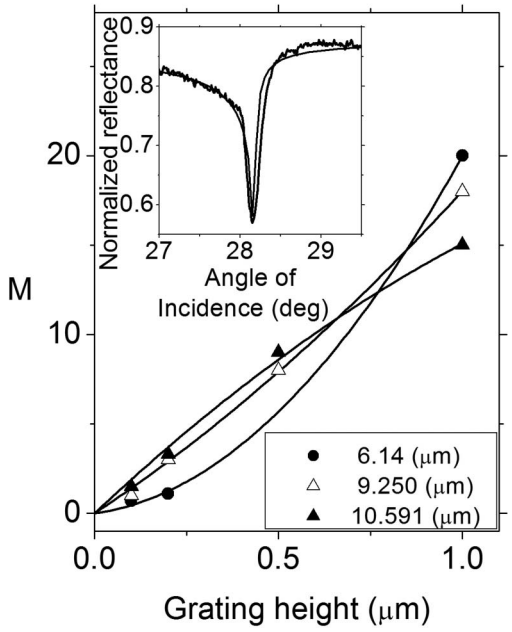

Fig. 7. Surface-impedance modulation parameter M (symbols) determined from fit of theory to observed resonances for grating amplitudes up to 1 μm. Solid curves are quadratic fits. (inset) Measured (thick curve) angular reflectance spectra for Ag grating of 0.5 μm amplitude at 10.591 μm wavelength compared with a best fit calculated spectrum (thin curve).

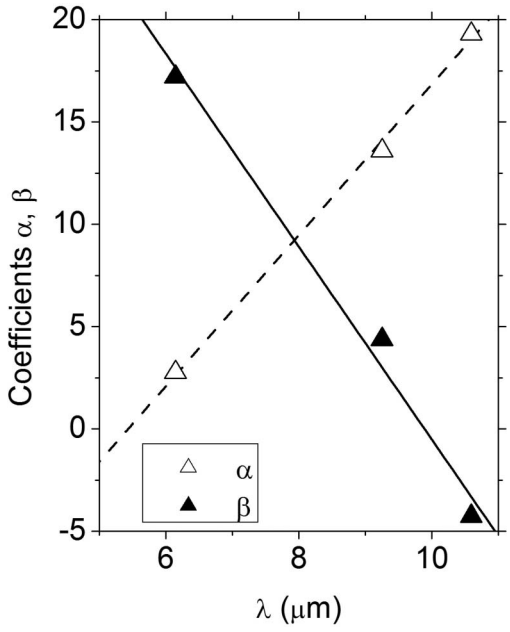

Fig. 8. Coefficients α and β plotted as a function of wavelength (symbols). Linear fitting of these values of the form of Eq. (21) are plotted (solid lines).

Figure 7 presents the fit values of the surface-impedance modulation parameter M as a function of the grating amplitude. Uncertainty in M values is smaller than the symbol size, except for the 1 μm gratings, where the uncertainty is ~10%. M values for the 6.14 μm wavelength are also included. For $h > 1$ μm, the distortion of the observed resonances and increasing disagreement between calculated and observed line shapes leads to larger uncertainty, so these data are left out of the Fig. 7 fits. Two effects are clear in Fig. 7. The surface-impedance modulation depends nonlinearly on grating amplitude, and it depends on the IR wavelength. The curves in Fig. 7 are fits of the function

$$M(h,\lambda) = \alpha(\lambda)h \ + \ \beta(\lambda)h^2. \qquad (20)$$

Fit values of α and β are given in Table 2.

Figure 8 shows that the coefficients α and β are nearly linear functions of λ. Curves in Fig. 8 are fits to the functions

$$\alpha(\lambda) = a_0 + a_1\lambda \qquad \beta(\lambda) = b_0 + b_1\lambda, \qquad (21)$$

where a_0, a_1, b_0, and b_1 have values of –20.0 μm^{-1}, 3.69 μm^{-2}, 46.6 μm^{-2}, and –4.71 μm^{-3} respectively.

Substituting Eq. (21) into Eq. (22) gives a function for the modulation parameter:

$$M(h,\lambda) = (a_0 + a_1\lambda)\ h + (b_0 + b_1\lambda)\ h^2. \qquad (22)$$

Thus, an empirical formula for the surface-impedance modulation parameter $M(h,\lambda)$ has been found for silver lamellar gratings in the mid-IR to LWIR. Figure 9 presents a contour plot of empirical M values. At short wavelengths, M increases more rapidly with h than at larger wavelengths. This simple form for the modulation index appears useful for grating heights up to ~15% of the IR wavelength.

Table 2. Fitting Parameters for M Versus h, according to Eq. (20)[a]

$\lambda(\mu m)$	$\alpha(\lambda)(\mu m^{-1})$	$\beta(\lambda)(\mu m^{-2})$
6.14	2.76	17.2
9.250	13.6	4.38
10.591	19.3	–4.26

[a]The largest grating amplitude data point used in the linear fits was 1 μm.

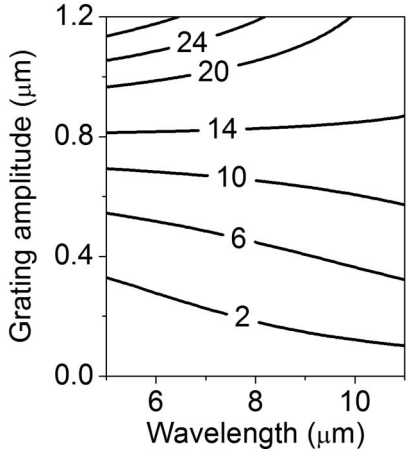

Fig. 9. Contour plot of M calculated for Ag gratings as a function of wavelength and grating amplitude.

5. Discussion

Measured resonance angles deviate from the calculated ones as the grating amplitude is increased. However, this shift amounts to only a few tenths of a degree at the maximum grating height that still gives a deep well-defined resonance. The shift may, therefore, be considered a secondary effect in the design and optimization of an SPP coupler, where the primary consideration is photon-to-SPP energy conversion.

The observed shift in Fig. 4 toward the calculated angles for the annealed 1 μm grating is likely due to the 30% reduction in its amplitude to a value that should give an angular deviation of only ~0.1°. An effect on the angles due to the change in profile from rectangular to sinusoidal need not be invoked. The higher harmonics involved in a rectangular profile lead mainly to higher order SPP resonances.

Though the theory [12] predicts no shift in resonance angle with grating amplitude, in contrast to the clear observations reported here and by others [4,5], and though we have concluded that such shifts are of secondary importance, there is at least a semiempirical way to account for them. The theory depends on the complex permittivity, which may be replaced by an effective permittivity for structured metals. For $n = 1$, we take the positive sign in Eq. (19), and an increase in k_{spp} causes an increase in the resonance angle θ, as observed for the $n = 1$ resonances in Fig. 5 when the grating amplitude is increased. If $n = -3$, we take the negative sign in Eq. (19), and an increase in k_{spp} leads to a decrease in θ as is observed in Fig. 5 for $n = -3$ with increasing h. Thus, observed angular shifts can be adequately explained by shifts in the SPP dispersion curve toward higher wavevector values with increasing grating amplitude, as reported in [4] for e-beam excited SPPs at visible frequencies on sinusoidal Ag gratings. According to Eq. (19), if ε is reduced, then k_{spp} moves to larger values further from the light line ($k = c/\omega$). Thus, the observed shift in resonance angles can be explained by a reduction in the permittivity as the surface becomes more and more structured and porous. A reduction in effective permittivity for a structured metal makes intuitive sense and has precedent [21], though it is possible to explain the shifts without such reductions by numerical methods [13–16].

There appears to be no clear theoretical relationship between the surface-impedance modulation parameter M and the experimental parameters h and λ. Neviere and Vincent [22] give a relation for the grating surface impedance that is proportional to $(h/\lambda)\ \cos^2(\theta)$ if $h \ll \lambda/\pi$. This fails to account for the observed curvature [Fig. 7]. Moreover, the linear dependence on wavelength that we find is not in agreement with a λ^{-1} dependence.

Wirgin and Maradudin [23] give a surface-impedance function Z that depends on λ, h, d, grating duty, and θ. However, their modulation parameter M is not a function of h, but instead the grating duty cycle and d. Depine and Brudny [24] give a simple relation $M = h/d$ for the modulation parameter in the Hessel and Oliner [12] surface-impedance model. This lacks curvature with h, and it has no λ dependence, in contrast to what is expected [12] or observed. References [12,22,23] indicate that SPP resonances are observable in reflection gratings only when the grating amplitude $h < \lambda/[4\cos(\theta)]$. For our CO_2 laser wavelengths (9.250, 10.591 μm) and the angle of resonance for the first order, the limiting amplitude is about 3 μm, which is in reasonable agreement with the value $h = 2$ μm, where the observed resonances become strongly deformed.

At the LWIR wavelengths studied, we found, both experimentally and theoretically, that the optimum grating amplitude that gave the deepest well-defined resonance was about 10%–15% of the wavelength. The resonances were much weaker at a 5% grating amplitude. This contrasts with [13], which reported that in the visible on sinusoidal gold gratings, the optimum h/λ was in the range of 3%–6% and decreased as the wavelength increased. We doubt that there is a fundamental difference in the behavior of sinusoidal and lamellar gratings, as each of the Fourier components for the latter appears to be acting independently, and the resonances due to each are well separated in the spectrum. It appears instead that in transitioning an SPP coupler to the LWIR, it is insufficient to merely scale all grating dimensions according to wavelength.

In conclusion, we have presented an approximate analytic formula for use in the design of SPP grating couplers. This approach relies on an impedance modulation parameter, which we have determined empirically by fitting the measured coupling of photons to SPPs for silver lamellar gratings at 6–11 μm wavelengths. The dependence of the surface-impedance modulation amplitude on wavelength and grating amplitude agrees poorly with the published expressions. Therefore, without an accurate theory for the dependence of the impedance modulation parameter on wavelength, material, and grating amplitude, a phenomenological dependence must be established so that the approach may be applied widely to the optimization of grating couplers.

This work was supported by the Air Force Office of Scientific Research under contracts FA8718-07C-0036, FA8718-06-C-0076, FA95500810428, and FA95501010030 (Gernot Pomrenke).

References

1. T. W. Ebbesen, C. Genet, and S. I. Bozhevolnyi, "Surface-plasmon circuitry," Phys. Today **61**, 44–50 (2008).
2. J. W. Cleary, R. E. Peale, D. Shelton, G. Boreman, and W. R. Buchwald, "Silicides for infrared surface plasmon resonance biosensors," Proc. Mater. Res. Soc. **1133**, 1133-AA10-03 (2008).
3. R. Soref, R. E. Peale, and W. R. Buchwald, "Longwave plasmonics on doped silicon and silicides," Opt. Express **16**, 6507–6514 (2008).
4. D. Heitmann, "Radiative decay of surface plasmons excited by fast electrons on periodically modulated silver surfaces," J. Phys. C: Solid State Phys. **10**, 397–405 (1977).

5. I. Pockrand, "Resonance anomalies in the light intensity reflected at silver gratings with dielectric coatings," J. Phys. D: Appl. Phys. **9**, 2423–2432 (1976).
6. M. C. Hutley and V. M. Bird, "A detailed experimental study of the anomalies of a sinusoidal diffraction grating," J. Mod. Opt. **20**, 771–782 (1973).
7. R. W. Day, S. S. Wang, and R. Magnusson, "Filter-response line shapes of resonant waveguide gratings," J. Lightwave Technol. **14**, 1815–1824 (1996).
8. F. J. Garcia-Vidal and L. Martin-Moreno, "Transmission and focusing of light in one-dimensional periodically nanostructured metals," Phys. Rev. B. **66**, 155412 (2002).
9. A. V. Kats and A. Y. Nikitan, "Nonzeroth-order anomalous optical transparency in modulated metal films owing to excitation of surface plasmon polaritons: an analytic approach," JETP Lett. **79**, 625–631 (2004).
10. D. Rosenblatt, A. Sharon, and A. A. Friesem, "Resonant grating waveguide structures," IEEE J. Quantum Electron. **33**, 2038–2059 (1997).
11. D. Shin, Z. S. Liu, and R. Magnusson, "Resonant Brewster filters with absentee layers," Opt. Lett. **27**, 1288–1290 (2002).
12. A. Hessel and A. A. Oliner, "A new theory of Wood's anomalies on optical gratings," Appl. Opt. **4**, 1275–1297 (1965).
13. M. C. Hutley and D. Maystre, "The total absorption of light by a diffraction grating," Opt. Commun. **19**, 431–436 (1976).
14. R. C. McPhedran and D. Maystre, "Detailed theoretical study of the anomalies of a sinusoidal diffraction grating," J. Mod. Opt. **21**, 413–421 (1974).
15. D. Maystre and M. Neviere, "Quantitative theoretical study on the plasmon anomalies of diffraction gratings," J. Opt. **8**, 165–174 (1977).
16. D. Maystre, "General study of grating anomalies from electromagnetic surface modes," in *Electromagnetic Surface Modes*, A. D. Boardman, ed. (Wiley, 1982), Chap. 17.
17. J. W. Cleary, R. E. Peale, D. J. Shelton, G. D. Boreman, C. W. Smith, M. Ishigami, R. Soref, A. Drehman, and W. R. Buchwald, "IR permittivities for silicides and doped silicon," J. Opt. Soc. Am. B **27**, 730–734 (2010).
18. Lord Rayleigh, "On the dynamical theory of gratings," Proc. R. Soc. London Ser. A **79**, 399–416 (1907).
19. R. W. Wood, "On a remarkable case of uneven distribution of light in a diffraction grating spectrum," Philos. Mag. **4**, 396–402 (1902).
20. H. Raether, *Surface Plasmons on Smooth and Rough Surfaces and on Gratings* (Springer, 1986).
21. S. Yang, "Effect of surface texture and geometry on spoof surface plasmon dispersion," Opt. Eng. **47**, 029001 (2008).
22. M. Neviere, P. Vincent, and R. Petit, "Some studies on behavior of surface impedance in vicinity of gratings," Opt. Commun. **21**, 369–373 (1977).
23. A. Wirgin and A. A. Maradudin, "Resonant response of a bare metallic grating to S-polarized light," Prog. Surf. Sci. **22**, 1–99 (1986).
24. R. A. Depine and V. L. Brudny, "A simple-model for a micro-rough diffraction grating that predicts diffuse light bands," J. Mod. Opt. **36**, 1257–1271 (1989).